Enhancements of the $\frac{3}{2}$ and $\frac{5}{2}$ frequencies of de Haas–van Alphen oscillations near the Lifshitz transition in a two-dimensional compensated metal with overtilted Dirac cones

Keita Kishigi
Faculty of Education, Kumamoto University, Kurokami 2-40-1, Kumamoto 860-8555, Japan

Yasumasa Hasegawa
Department of Material Science, Graduate School of Material Science, University of Hyogo, Hyogo 678-1297, Japan

(Received 17 June 2019; published 25 November 2019)

We study the de Haas-van Alphen (dHvA) oscillations in the two-dimensional compensated metal with overtilted Dirac cones near the Lifshitz transition. We employ the tight-binding model of α-(BEDT-TTF)$_2$I$_3$, in which the massless Dirac fermions are realized. When a uniaxial pressure (P) along the y axis is applied above $P \simeq 0.2$ kbar in α-(BEDT-TTF)$_2$I$_3$, one electron pocket, which encloses the overtilted Dirac points, is changed to two electron pockets, i.e., Lifshitz transition happens, while a hole pocket does not change a topology. We show that the Fourier components corresponding to the $\frac{3}{2}$ and $\frac{5}{2}$ areas of the hole pocket are anomalously enhanced in the region of pressure where the Lifshitz transition occurs. This phenomenon will be observed in the two-dimensional overtilted Dirac fermions near the Lifshitz transition.

DOI: 10.1103/PhysRevB.100.195433

I. INTRODUCTION

The de Haas van Alphen (dHvA) oscillations are the phenomena that the magnetization in metals oscillates periodically as a function of the inverse of the magnetic field ($1/H$) at low temperatures [1]. Lifshitz and Kosevich [2] have derived semiclassically the standard formula called the LK formula [1–3], which is Eq. (A1) in Appendix A. The fundamental frequency of the dHvA oscillations corresponds to the extremal cross-sectional area of the Fermi surface perpendicular to the applied field.

When the distance between two parts of a Fermi surface is narrow and the energy barrier between them is not high, electrons can tunnel from one part of the Fermi surface to another in the magnetic field, which is called the magnetic breakdown. In that case, a new period of the dHvA oscillations appears, which corresponds to the area of the effective closed orbit of electrons. The dHvA oscillations in the system with magnetic breakdown have been studied in the semiclassical network model [4,5], in which the probability amplitudes of the tunneling are introduced into the LK formula as parameters. The phenomenological probability amplitudes, however, are not necessary to be introduced into the quantum-mechanical treatment in the tight-binding model, as we will show in this paper.

When the system has a three-dimensional Fermi surface (for example, a sphere), the kinetic energy perpendicular to the magnetic field is quantized as Landau levels and the kinetic energy parallel to the magnetic field is not affected. In that case, the chemical potential changes little as a function of the magnetic field. Then we can use the LK formula, neglecting the magnetic-field dependence of the chemical potential. In two-dimensional systems or quasi-two-dimensional systems with the interlayer coupling smaller than the spacings of the Landau levels, however, the magnetic-field dependence of the chemical potential cannot be neglected in general, and the LK formula assuming the fixed chemical potential is not justified. In simple systems with two-dimensional free electrons, the sawtooth pattern of the dHvA oscillations is inverted depending on whether we fix the chemical potential or electron number, although the frequency of the dHvA oscillations is the same [1,6,7]. When the quasi-two-dimensional system has two or more Fermi surfaces [electron pocket(s) and hole pocket as studied in this paper, or two-dimensional Fermi pocket and quasi-one-dimensional (open) Fermi surface], the oscillation of the chemical potential as a function of the inverse magnetic field causes the "*forbidden*" frequencies such as $f_\beta - f_\alpha$ [8–14]. The forbidden frequencies in the dHvA oscillations have been studied theoretically in systems with isolated Fermi surfaces (without the magnetic breakdown) [15–21] and with Fermi surfaces connected by the magnetic breakdown [9,22–28].

We have studied the energy of the quasi-two-dimensional organic conductor, α-(BEDT-TTF)$_2$I$_3$ [29–31], in the external magnetic field at various uniaxial pressure in the recent paper [32]. We found that the magnetic-field dependence of the Landau levels is proportional to $H^{4/5}$ at the pressure when the Dirac cone is tilted critically (three-quarter Dirac points), i.e., the linear term disappears and the quadratic term becomes dominant in one direction, while the linear term is finite in the other three directions [32,33]. The Dirac cone is undertilted when the pressure is higher than the critical pressure (2.3 kbar) and it is overtilted when the pressure is lower. Even at the critical pressure where the three-quarter Dirac points are realized, the Fermi energy is higher than the energy at the three-quarter Dirac point, since the three-quarter Dirac point is not the local maximum of the lower band due to the positive quadratic term. As a result, the system is a compensated metal

with one hole pocket around the maximum of the lower band and two electron pockets surrounding two Dirac points below 3.0 kbar. It is known that the phase (γ) [34–36] in the dHvA oscillations is $1/2$ in the topologically trivial parabolic band (hole pocket in our case) but $\gamma = 0$ due to the Berry phase π in the Dirac fermions (electron pockets in our case).

The dHvA oscillations in the two-dimensional compensated metallic state have been studied semiclassically [37,38] and quantum mechanically [39,40] in the systems such as $(TMTSF)_2NO_3$ [41–43], where there are one hole pocket and one electron pocket with the same area. In these studies, both the free hole pocket and the free electron pocket are topologically trivial. The compensated metallic state of α-$(BEDT\text{-}TTF)_2I_3$ is a unique system, because there are a coexisting trivial hole pocket and one or two electron pockets with Dirac-fermion property near the Lifshitz transition [44,45]—a similar situation will be realized in the systems with overtilted Dirac points (type II Weyl semimetal) [46,47]. Therefore, it is interesting to study the dHvA oscillations near the Lifshitz transition in α-$(BEDT\text{-}TTF)_2I_3$. The semiclassical picture will be difficult to be applied in that system, since the density of states diverges at the Fermi surface when the Lifshitz transition happens [48].

In this paper, we study the dHvA oscillations at and near the Lifshitz transition in the two-dimensional compensated metal with a trivial hole pocket and two or one electron pocket(s) surrounding the overtilted Dirac points. We use the tight-binding model for α-$(BEDT\text{-}TTF)_2I_3$ with pressure-dependent transfer integrals. The effect of the magnetic field is taken into account by the Peierls substitution and we do not consider the semiclassical network model of the magnetic breakdown.

A main result in this study is shown in Fig. 1. The Fourier transform intensities (FTIs) for the $\frac{3}{2}$ and $\frac{5}{2}$ times of the area of a hole pocket are enhanced in the region of pressure, where the Lifshitz transition occurs, when we take the condition that the electron number is fixed, as shown in Fig. 1(a). When the chemical potential is fixed, these enhancements do not appear, as shown in Fig. 1(b).

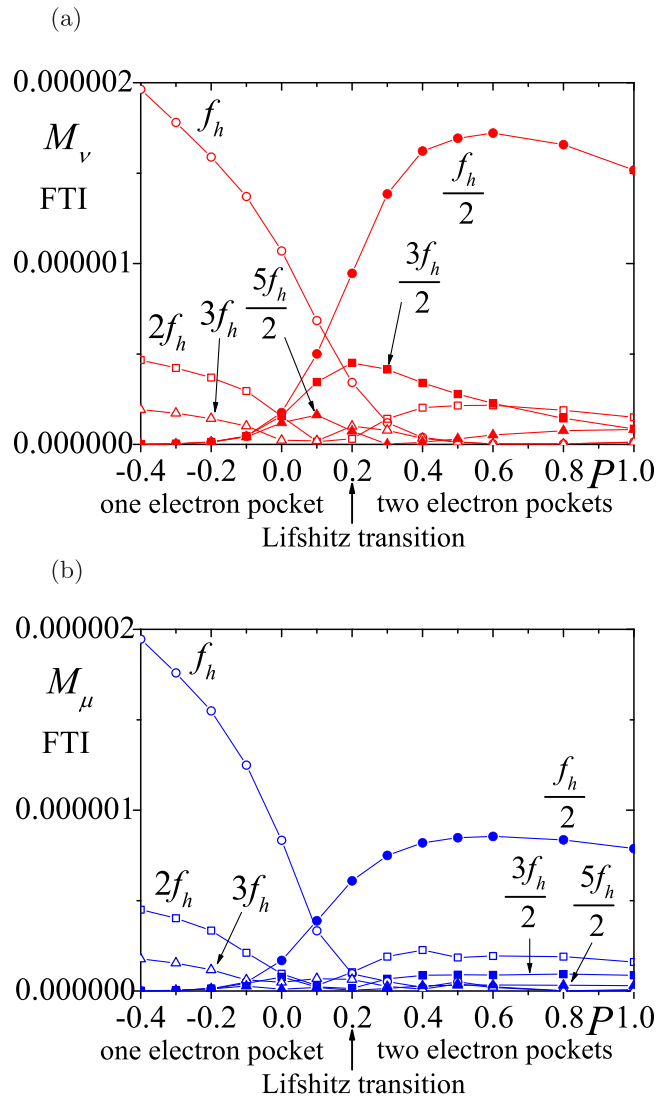

FIG. 1. The P-dependencies of the FTIs, where (a) and (b) are for M_ν in Fig. 9 and M_μ in Fig. 10, respectively. The Lifshitz transition occurs at $P = 0.2$. There exist one electron pocket and one hole pocket at $P < 0.2$, while there exist two electron pockets and one hole pocket at $P > 0.2$. Dirac cones are overtilted at $P < 2.3$.

II. TIGHT-BINDING MODEL FOR α-(BEDT-TTF)$_2$I$_3$; COMPENSATED METAL AND THE LIFSHITZ TRANSITION

α-$(BEDT\text{-}TTF)_2I_3$ [29,30,52] is known as one of quasi-two-dimensional organic superconductors. Due to the smallness of the interlayer coupling, we ignore the three-dimensionality of α-$(BEDT\text{-}TTF)_2I_3$. Four BEDT-TTF molecules exist in the unit cell, as shown in Fig. 2. The four energy bands are constructed by the highest occupied molecular orbits (HOMO) of BEDT-TTF molecules. Since one electron is removed from two BEDT-TTF molecules, the electron bands are $\frac{3}{4}$-filled. The lower two bands are completely filled by electrons. In this paper, the tight-binding model for the HOMO having the transfer integrals between neighboring sites is used, which is shown in Fig. 2. The tight-binding model has been explained in a previous study [32].

Although α-$(BEDT\text{-}TTF)_2I_3$ exhibits a metal-insulator transition due to the charge ordering at low temperatures and low pressures [53–56], we employ the model without interactions to study the effects of the Lifshitz transition. The charge-ordering phase in α-$(BEDT\text{-}TTF)_2I_3$ has been observed at $P \lesssim 3.0$ kbar under the uniaxial pressure along the x axis and $P \lesssim 5.0$ kbar along the y axis in the conductivity [57] and under the hydrostatic pressure at $P \lesssim 17$ kbar from the magneto conductivity [58] and at $P \lesssim 11 - 12$ kbar from the optical investigation [59] and conductivity [60]. Even in the field-induced charge-density-wave state, magnetic quantum oscillations have been observed in the similar system of α-$(BEDT\text{-}TTF)_2MHg(SCN)_4$ with $M =$ K and Tl [61].

Recently, massless Dirac fermions have been observed [62–66] in α-$(BEDT\text{-}TTF)_2I_3$ under the pressure. The appearance of the massless Dirac fermions has been theoretically shown by Katayama *et al.* [31]. They have used the interpolation formula [67] for the transfer integrals based on the

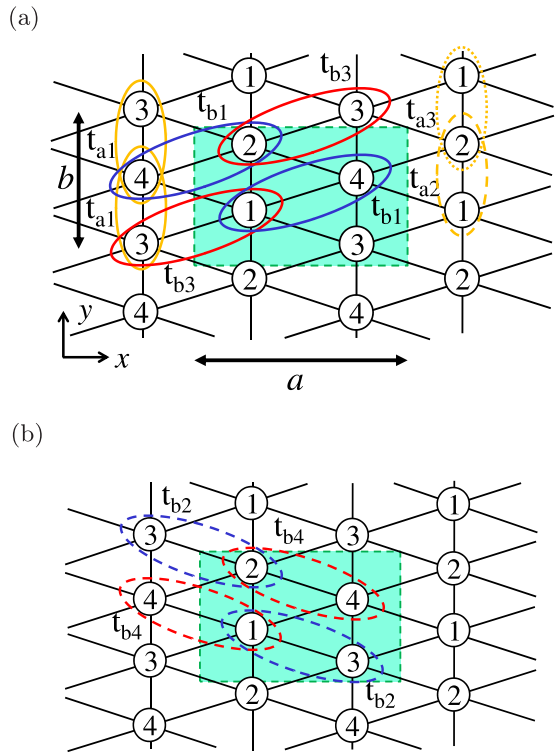

FIG. 2. The crystal lattice and the transfer integrals in the tight-binding model in α-(BEDT-TTF)$_2$I$_3$. The transfer integrals (t_{a1}, t_{a2}, t_{a3}, t_{b1}, t_{b2}, t_{b3}, and t_{b4}) are shown as ovals. The unit cell is the rectangle in (a) and (b), where a and b are the lattice constants along the x axis and y axis, respectively.

extended Hückel method [68,69]. These are given by

$$\begin{aligned} t_{a1} &= -0.028(1.0 + 0.089P), \\ t_{a2} &= -0.048(1.0 + 0.167P), \\ t_{a3} &= 0.020(1.0 - 0.025P), \\ t_{b1} &= 0.123, \\ t_{b2} &= 0.140(1.0 + 0.011P), \\ t_{b3} &= 0.062(1.0 + 0.032P), \\ t_{b4} &= 0.025, \end{aligned} \tag{1}$$

where P is the uniaxial strain along the y axis. Hereafter, we employ eV and kbar as the units of transfer integrals and the pressure, respectively. In this paper, we use Eqs. (1).

When $P \geqslant 3.0$, the Fermi energy is located at the Dirac points. A similar band structure has been shown in the first-principles band calculations by Kino and Miyazaki [70,71] and Alemany *et al.* [72].

At $P < 3.0$, the top of the third band from the bottom band becomes a higher energy than that at the Dirac points. In this case, there are one hole pocket and one or two electron pockets. For example, the Fermi surfaces at $P = -0.4$, 0, 0.2, and 1.0 are shown in Fig. 3, where the use of the negative P is allowed in Eqs. (1). We extrapolate the pressure to a negative value. The area of the hole pocket is the same as the sum of the areas of each electron pocket, i.e., the system is a compensated metal. The hole pocket has a parabolic dispersion around

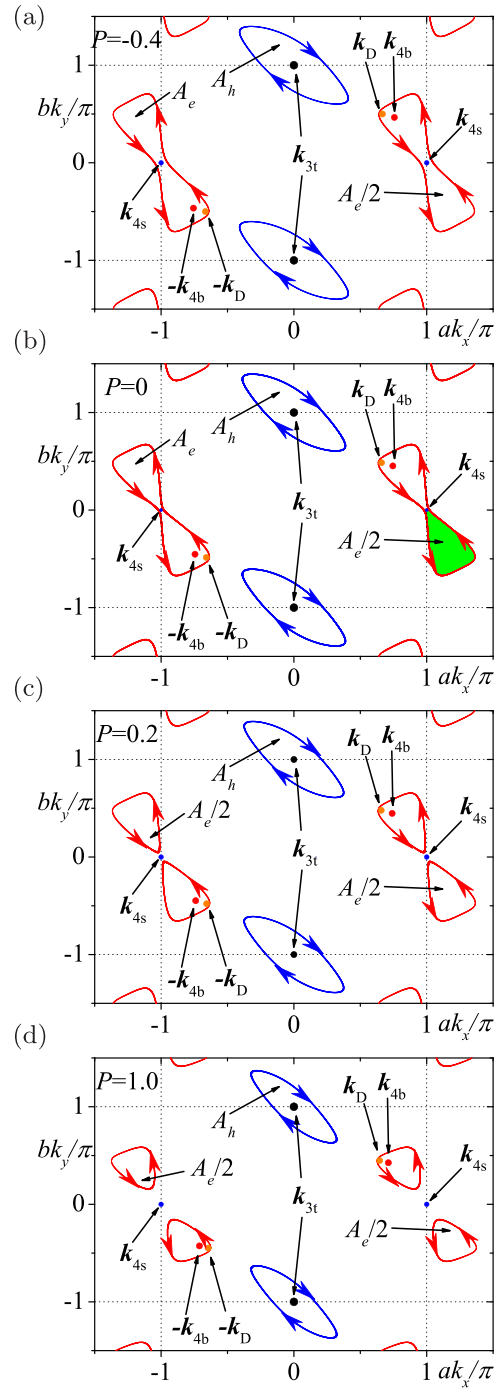

FIG. 3. Fermi surfaces at $P = -0.4$ (a), $P = 0$ (b), $P = 0.2$ (c), and $P = 1.0$ (d) in the extended zone, where $\mathbf{k}_{3t}$ is the wave vector for the top of the third band, $\pm\mathbf{k}_D$ are Dirac points, $\pm\mathbf{k}_{4b}$ are the points with the bottom energy in the fourth band, $\mathbf{k}_{4s}$ is the saddle point of the fourth band. Arrows indicate the direction of the orbital motion for electrons in the magnetic field in the semiclassical picture. In (b), a green area is a half of A_e. We obtain $|A_h|/A_{BZ} \simeq 0.0797$ at $P = -0.4$ (a), $A_e/A_{BZ} = |A_h|/A_{BZ} \simeq 0.0714$ at $P = 0$ (b), $|A_h|/A_{BZ} \simeq 0.0666$ at $P = 0.2$ (c), and $|A_h|/A_{BZ} \simeq 0.0480$ at $P = 1.0$ (d), where A_{BZ} is the area of the Brillouin zone, $|A_h|$ is the area of a hole pocket and A_e is the area of an electron pocket [(a) and (b)] or the sum of the area of two electron pockets [(c) and (d)]. Note that the sign of the area of the hole pocket is opposite of that of the electron pocket [5,37].

$\mathbf{k}_{3t}$. The saddle point exists near the Dirac points in the fourth band at $\mathbf{k}_{4s} = (\pi/a, 0)$. This point is the time-reversal invariant momentum (TRIM), which may become one of a local maximum point, a local minimum point, an inflection point, or a saddle point. This is explained in Appendix C.

The densities of states at $P = -0.4, 0, 0.2$, and 1.0 are shown in Fig. 4. We can see the logarithmic divergence caused by the fourth band. The divergence near the Fermi energy at $P = 0$ and 0.2 are due to the saddle point at $\mathbf{k}_{4s}$. The peak of the density of states crosses the Fermi energy at the pressure of the Lifshitz transition.

III. ENERGY IN THE MAGNETIC FIELD

We study the case that the uniform magnetic field is applied perpendicular to the $x - y$ plane. We neglect spins for simplicity. If we consider the effect of spin, it has been known the amplitudes for some frequencies in the fixed electron number are different from those of LK formula [73].

We take the ordinary Landau gauge

$$\mathbf{A} = (Hy, 0, 0). \tag{2}$$

The flux through the unit cell is given by

$$\Phi = abH, \tag{3}$$

where a and b are the lattice constants. We use the Peierls substitution as done before [32]. We obtain numerical solutions when the magnetic field is commensurate with the lattice period, i.e.,

$$\frac{\Phi}{\phi_0} = \frac{p}{q} \equiv h, \tag{4}$$

where $\phi_0 = 2\pi\hbar c/e \simeq 4.14 \times 10^{-15}$ Tm^2 is a flux quantum, e is the absolute value of the electron charge ($e > 0$), c is the speed of light, $\hbar$ is the Planck constant divided by 2π, and p and q are integers. Hereafter, we represent the strength of the magnetic field by h of Eq. (4). Since $a \simeq 9.211$ Å and $b \simeq 10.85$ Å in α-(BEDT-TTF)$_2$I$_3$ [29], $h = 1$ corresponds to $H \simeq 4.14 \times 10^3$ T.

At $P = -0.4$, the energies near the Fermi energy are shown in Fig. 5. At the higher field ($h \gtrsim 0.010$), the broadening of the Landau levels (the Harper broadening [74]) are seen. These broadenings are very small at the lower field ($h \lesssim 0.010$). Thus, the energies at the low field regions can be understood in terms of the Landau quantization with no broadenings. Similar results are obtained from other pressure values such as $P = 0, 0.2$ and 1.0. Hereafter, we ignore the wave-number dependencies in the magnetic Brillouin zone along k_x and k_y, because the Harper broadening is negligibly small.

At the lower field ($h \leqslant 0.005$), the energies as a function of h at $P = -0.4, 0, 0.2$, and 1.0 are shown in Figs. 6(a)–6(d). We consider that the system is at the low temperature (T) much smaller than the spacing of the Landau levels. Then we take $T = 0$. The chemical potential (μ, i.e., the Fermi energy) changes as a function of h, when the electron number is fixed in the compensated metal without the electron-hole symmetry. Since all Landau levels for the electron pocket(s) and hole pocket have the same degeneracy at the fixed magnetic field, the numbers of occupied Landau levels for electrons and holes are the same in the compensated metal. The chemical potential is taken as the middle value between the energy of

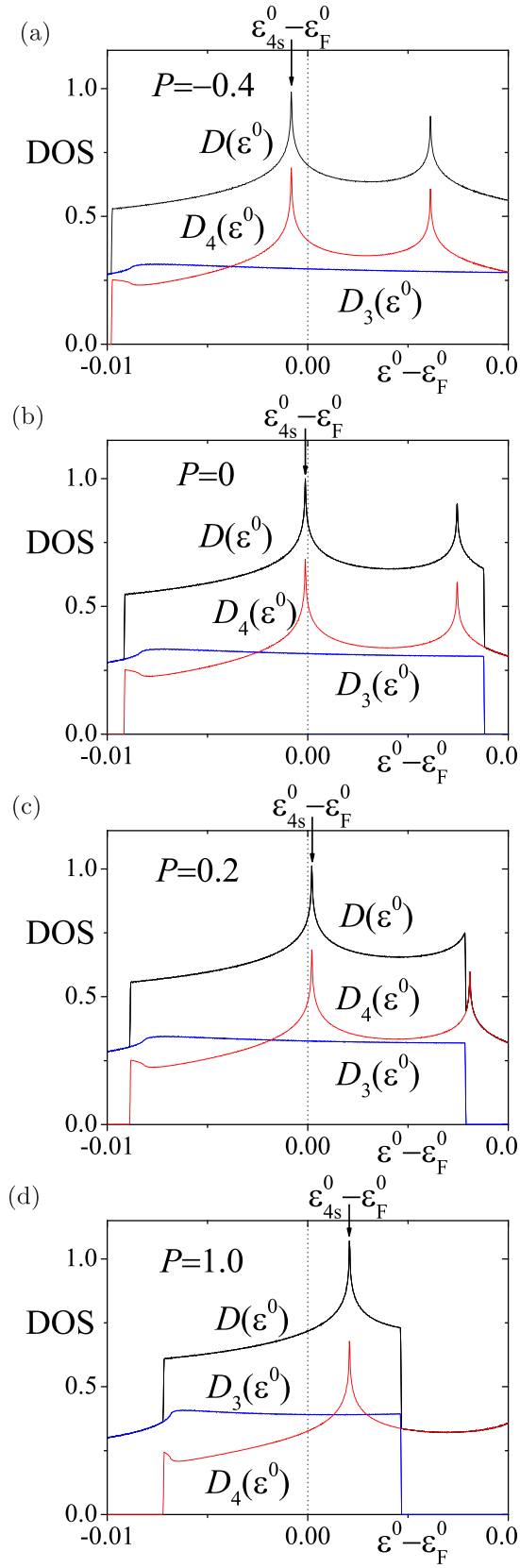

FIG. 4. Density of states $[D(\varepsilon^0)]$ at $H = 0$ as a function of the energy (ε^0) measured from ε^0_F (the Fermi energy at $H = 0$) at (a) $P = -0.4$, (b) $P = 0$, (c) $P = 0.2$, and (d) $P = 1.0$. The density of states originated from the fourth band (red lines) and third band (blue lines) are also plotted.

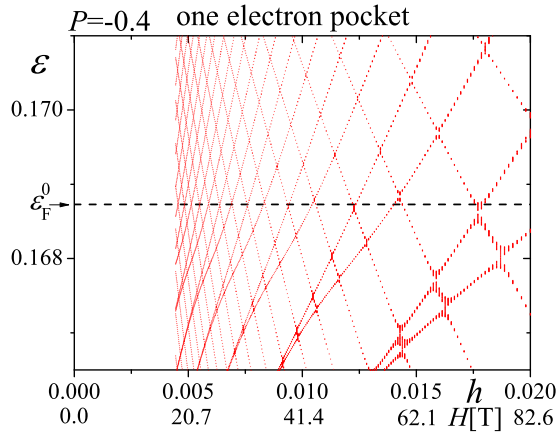

FIG. 5. Energies near the Fermi energy as a function of h at $P = -0.4$ (one electron pocket). We choose $p = 2$ and $100 \leqslant q \leqslant 450$ ($q = 100, 101, \ldots, 449, 450$). The magnetic Brillouin zones are $-\frac{\pi}{a} \leqslant k_x < \frac{\pi}{a}$ and $-\frac{\pi}{qb} \leqslant k_y < \frac{\pi}{qb}$. Since the energies are independent of the gauge of the vector potential, we set the increments in the magnetic Brillouin zone along k_x and k_y and are taken as $2\pi/(aq) \times 1/7$ and $2\pi/(bq) \times 1/5$, respectively. A black dotted line is $\varepsilon_{\rm F}^0$.

the highest occupied states and that of the lowest unoccupied state, as shown in blue lines in Fig. 6 as a function of h. Two Landau levels are effectively degenerated at the blue circles in Figs. 6(b)–6(d), although there are negligible energy gaps between them. This separation of the Landau levels is a quantum mechanical picture of the semiclassical magnetic breakdown. Montambaux *et al.* [75] have also studied the degeneracy and the separation of Landau levels in the model with two electron pockets.

The Landau levels and μ at $h = 0.00475$ [dotted green lines in Figs. 6(a), 6(c) and 6(d)] are shown in Figs. 7(a)–7(c), respectively, where n is the index of Landau levels. The Landau levels with $n = 11$ and 12 at $P = 0.2$ [Fig. 7(b)] and those with $n = (7, 8)$, (9,10), and (11,12) at $P = 1.0$ [Fig. 7(c)] are degenerated or effectively degenerated, which can be interpreted as the Landau quantization of almost-independent two electron pockets in a semiclassical picture. The degeneracy of the Landau levels with $n = 13$ and 14 at $P = 0.2$ is lifted [Figs. 6(c) and 7(b)], which can be understood as a result of weakly coupled two electron pockets near the Fermi energy as shown in Fig. 3(c).

We show $\mu - \varepsilon_{\rm F}^0$ at $P = -0.4$, 0, 0.2, and 1.0 in Fig. 8. Since the symmetry of the electron band and the hole band near the Fermi energy is not bad at $P = -0.4$ [see Fig. 6(a)], the h dependence of μ is small, as shown in Fig. 8(a). However, the electron-hole symmetry becomes worse as P increases, as shown in Figs. 6(a)–6(d). Therefore, as P increases, the amplitude of the oscillation of μ increases, as shown in Fig. 8.

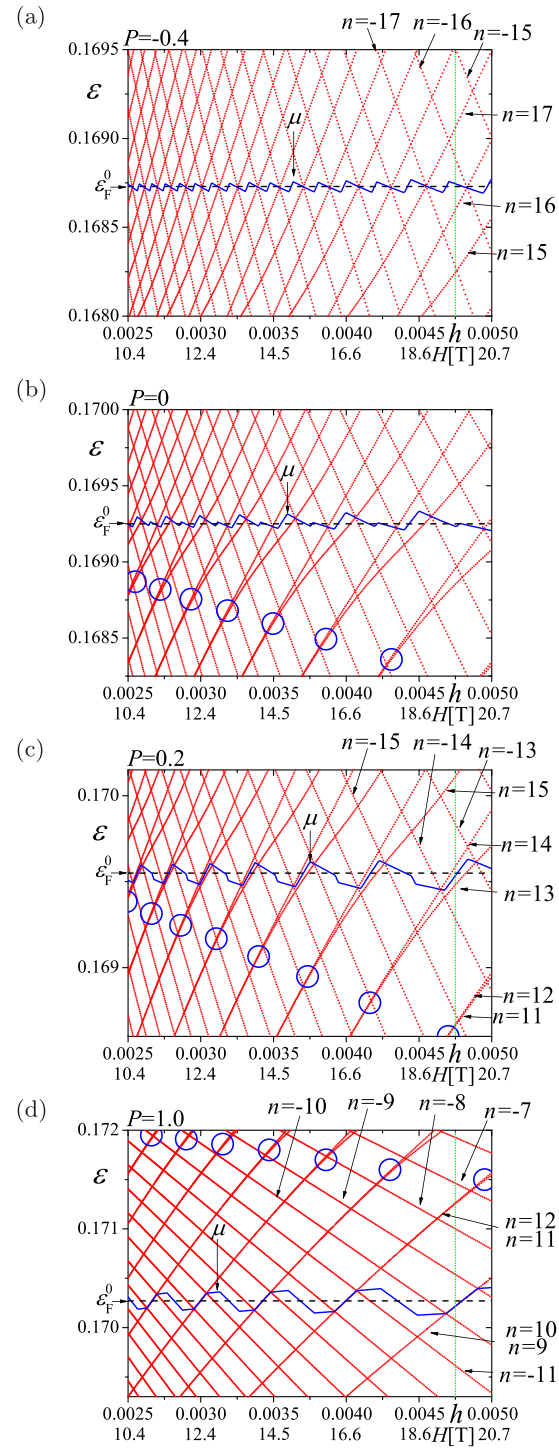

FIG. 6. Energies near the Fermi energy as a function of h at $P = -0.4$ (a), $P = 0$ (b), $P = 0.2$ (c), and $P = 1.0$ (d). The region of the magnetic field is smaller than that in Fig. 5, where we take $p = 2$ and $400 \leqslant q \leqslant 800$ ($q = 400, 401, \ldots, 799, 800$). We indicate $\varepsilon_{\rm F}^0$ at $h = 0$ by the black broken lines and μ at $h \neq 0$ in fixed ν by the blue lines, respectively. Blue circles indicate the effective merging points of two Landau levels for electron pockets.

IV. TOTAL ENERGY AND MAGNETIZATION IN THE MAGNETIC FIELD

In this section, we explain the calculations of the total energy and magnetization as a function of external magnetic field in two situations; one is the case of the fixed electron number and the other is the case of the fixed chemical potential. The first case, the fixed electron number or fixed electron filling to be $\frac{3}{4}$, is plausible in the isolated

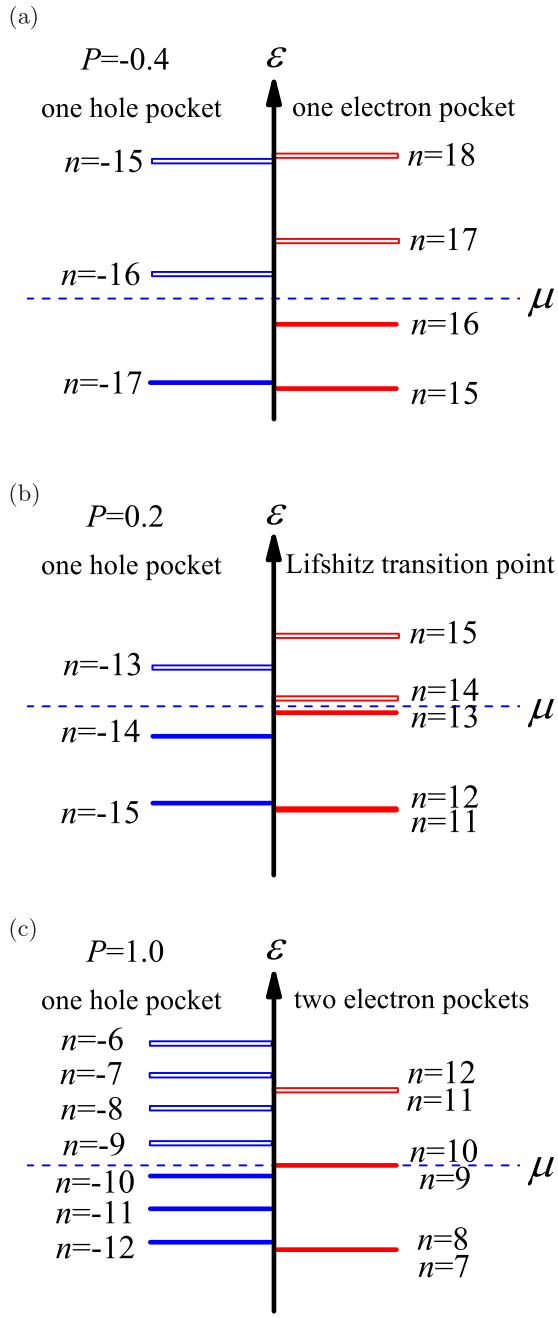

FIG. 7. (a)–(c) are the Landau levels at $P = -0.4$, 0.2 and 1.0 at $h = 0.00475$ [dotted green lines in Figs. 6(a), 6(c) and 6(d)], respectively. Filled red (blue) boxes are for the completely occupied electron's (hole's) Landau levels, and blank red (blue) boxes are for the unoccupied electron's (hole's) Landau levels, respectively.

two-dimensional systems [1,6,7,9,15,17,24]. The fixed chemical potential is realized if there exist the electron reservoirs, the three-dimensionality, or the thermal broadening.

At $T = 0$, the total energy (E_ν) under the condition of the fixed electron number [i.e., the fixed electron filling (ν)] is calculated by

$$E_\nu = \frac{1}{4qN_k} \sum_{i=1}^{4qN_k\nu} \varepsilon(i, \mathbf{k}), \tag{5}$$

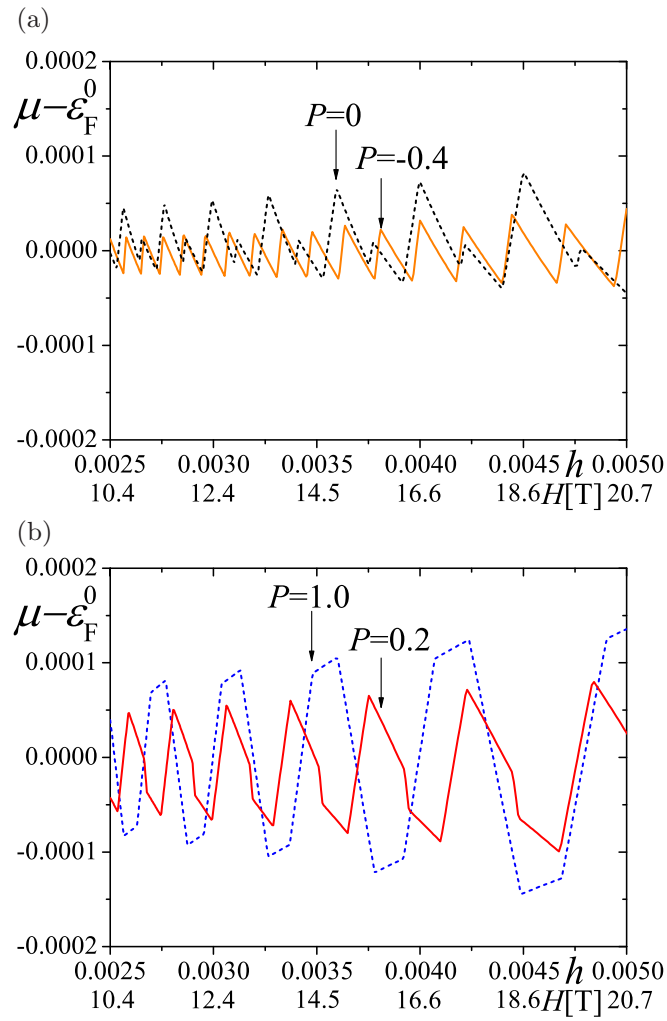

FIG. 8. The chemical potential μ for the $\frac{3}{4}$-filling as a function of h at $P = -0.4$ and 0 (a) and at $P = 0.2$ and 1.0 (b).

where N_k is the number of $\mathbf{k}$ points taken in the magnetic Brillouin zone. In this system, $\nu = 3/4$.

The total energy (E_μ) under the condition of fixed μ is calculated by

$$E_\mu = \frac{1}{4qN_k} \sum_{\varepsilon(i,\mathbf{k}) \leqslant \mu} (\varepsilon(i, \mathbf{k}) - \mu), \tag{6}$$

where $4q$ is the number of bands in the presence of magnetic field, and $\varepsilon(i, \mathbf{k})$ is the eigenvalues of $4q \times 4q$ matrix. The fixed chemical potential in Eq. (6) is given by

$$\mu = \varepsilon_{\mathrm{F}}^0, \tag{7}$$

where $\varepsilon_{\mathrm{F}}^0$ is the Fermi energy at $h = 0$.

We have checked that if q is large enough as taken in the present paper, the wave-number dependence of the eigenvalues $\varepsilon(i, \mathbf{k})$ is very small. Therefore, we can take $N_k = 1$.

The magnetizations for fixed ν and fixed μ are numerically obtained by

$$M_\nu = -\frac{E_\nu(h + \Delta h) - E_\nu(h)}{\Delta h}, \tag{8}$$

$$M_\mu = -\frac{E_\mu(h + \Delta h) - E_\mu(h)}{\Delta h}, \tag{9}$$

respectively. If the h dependence of μ is negligibly small, we obtain

$$M_\nu = M_\mu. \tag{10}$$

V. DE HAAS VAN ALPHEN OSCILLATIONS AND ITS PRESSURE DEPENDENCE

At $P = -0.4$, the wave form of M_ν of Fig. 9(a) is almost the same as that of M_μ of Fig. 10(a), because the h dependence of μ is very small [see Fig. 8(a)]. The sawtooth shapes of M_ν and M_μ are the same as that of the LK formula. As P increases, the amplitude of the oscillation of μ increases [see Figs. 8(a) and 8(b)], and the wave forms of M_ν at $P = 0$, 0.2, and 1.0 deviate from those of M_μ, as shown in Figs. 9(b)–9(d) and Figs. 10(b)–10(d).

We show an enlarged view of Fig. 6(a) at $P = -0.4$ in Fig. 11(a), where the crossing points (green arrows) of the Landau levels (red dotted lines) and μ (a blue line) are almost the same as those (black arrows) of the Landau levels and $\varepsilon_{\rm F}^0$ (a dotted black line). The jumps of M_ν and M_μ also occur at these crossing points, as shown in Fig. 11(b). We show the enlarged views of Figs. 6(b)–6(d) at $P = 0$, 0.2, and 1.0 in Figs. 12(a), 13(a), and 14(a). In Figs. 11(a), 12(a), 13(a), and 14(a), μ always intersects the points where the occupied electron's Landau levels and the unoccupied hole's Landau levels cross. The crossing points (green arrows) of the Landau levels and μ are different from those (black arrows) of the Landau levels and $\varepsilon_{\rm F}^0$. The jumps of M_ν and M_μ happen at green arrows and black arrows, respectively, as shown in Figs. 12(b), 13(b), and 14(b).

The FTIs of M_ν and M_μ are shown in Fig. 15 at $P = -0.4$, 0, 0.2, and 1.0. When $P = -0.4$, there are peaks at $f_h \simeq 0.0798$ and the higher harmonics ℓf_h, and they are proportional to $1/\ell$ [blue dotted line in Fig. 15(a)]. This is due to the sawtooth waveform of M_ν and M_μ [see Fig. 11(b)]. The value of f_h corresponds to the area of an electron pocket and a hole pocket ($A_e/A_{\rm BZ} = |A_h|/A_{\rm BZ} \simeq 0.0797$), as shown in Fig. 3(a). This coincidence is expected in the LK formula. Furthermore, the FTIs at $f_h, 2f_h, 3f_h, \ldots, lf_h, \ldots$ are well fitted by the LK formula [Eq. (B2)] [blue diamonds in Fig. 15(a)], where the value of the FTI at f_h in M_μ is used as $M_0 A_e$. In that fitting, the amplitude modified by the network model is not used. Thus, at $P = -0.4$ and 10.4 T $\leqslant H \leqslant$ 20.7 T, we can neglect the interband coupling by the magnetic breakdown.

At $P = 0$, there are the peaks at $f_h \simeq 0.0714$, $2f_h$ and $3f_h$ in the FTIs of Fig. 15(b), where f_h corresponds to the area of an electron pocket and a hole pocket ($A_e/A_{\rm BZ} = |A_h|/A_{\rm BZ} \simeq 0.0714$), as shown in Fig. 3(b). These peaks are expected in the LK formula. In addition, we can see the peaks at $f_h/2$, $3f_h/2$, $5f_h/2$, and $7f_h/2$ in M_ν and M_μ, although there are no closed orbits with the areas corresponding to $f_h/2$, $3f_h/2$, $5f_h/2$, and $7f_h/2$. These peaks might be explained by the semiclassical network model with tuning tunneling parameters. For example, for the peaks at $f_h/2$ in M_ν and M_μ, an electron's effective closed orbital motion with the green area ($A_e/2 = |A_h|/2$) in Fig. 3(b) is possible by the tunneling thorough the narrow neck when the magnetic field is strong. Similarly, the small peaks at $3f_h/2$, $5f_h/2$, and $7f_h/2$ in M_μ and M_ν might be understood by the multitunneling [4,5].

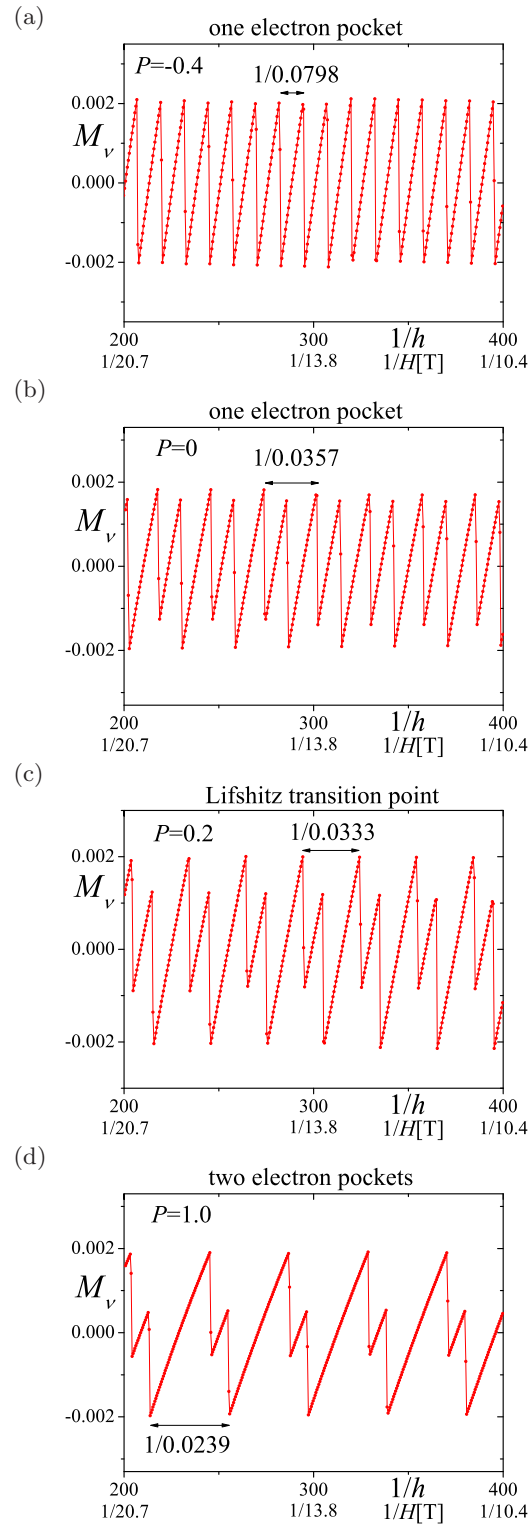

FIG. 9. Magnetization as a function of $1/h$ at $P = -0.4$ (one electron pocket) (a), $P = 0$ (one electron pocket) (b), $P = 0.2$ (Lifshitz transition point) (c) and $P = 1.0$ (two electron pockets) (d) obtained with fixed electron filling ν.

At $P = 0.2$, there are the peaks at $f_h \simeq 0.00667$, $2f_h$, $3f_h$, and $4f_h$ in M_ν and M_μ, as shown in Fig. 15(c). The value of f_h corresponds to the area of a hole pocket ($|A_h|/A_{\rm BZ} \simeq 0.0666$) or the sum of the area of two electron pockets ($A_e = |A_h|$), as

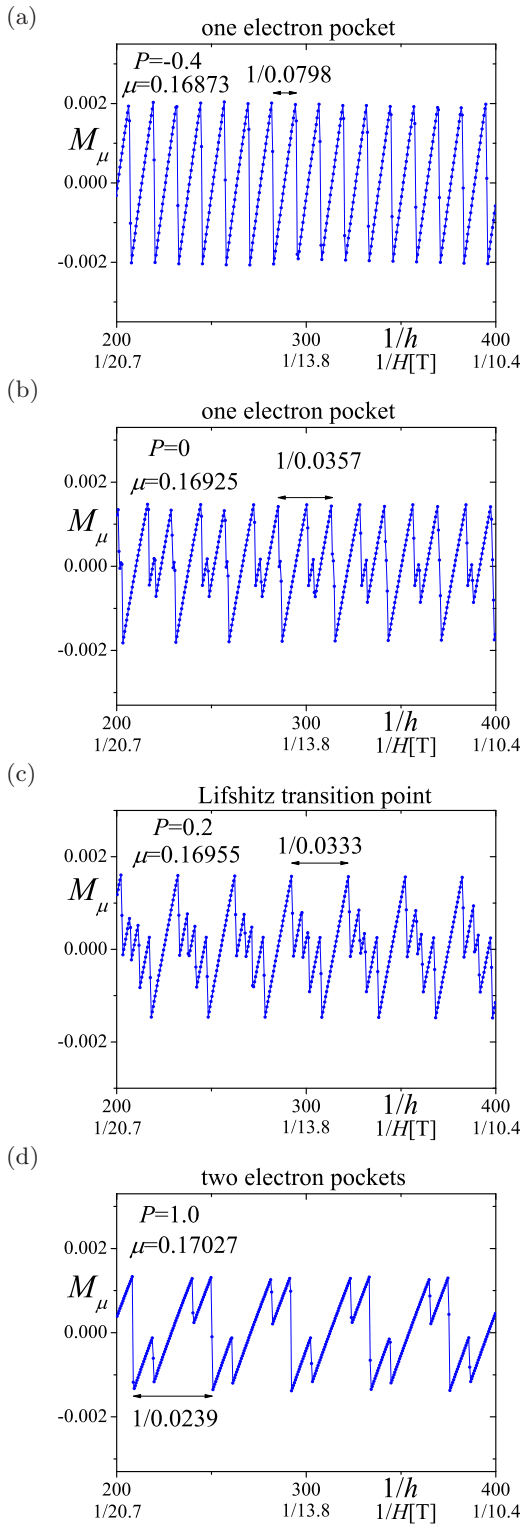

FIG. 10. Magnetization as a function of $1/h$ at $P = -0.4$ (one electron pocket) (a), $P = 0$ (one electron pocket) (b), $P = 0.2$ (Lifshitz transition point) (c), and $P = 1.0$ (two electron pockets) (d) obtained with fixed chemical potential μ.

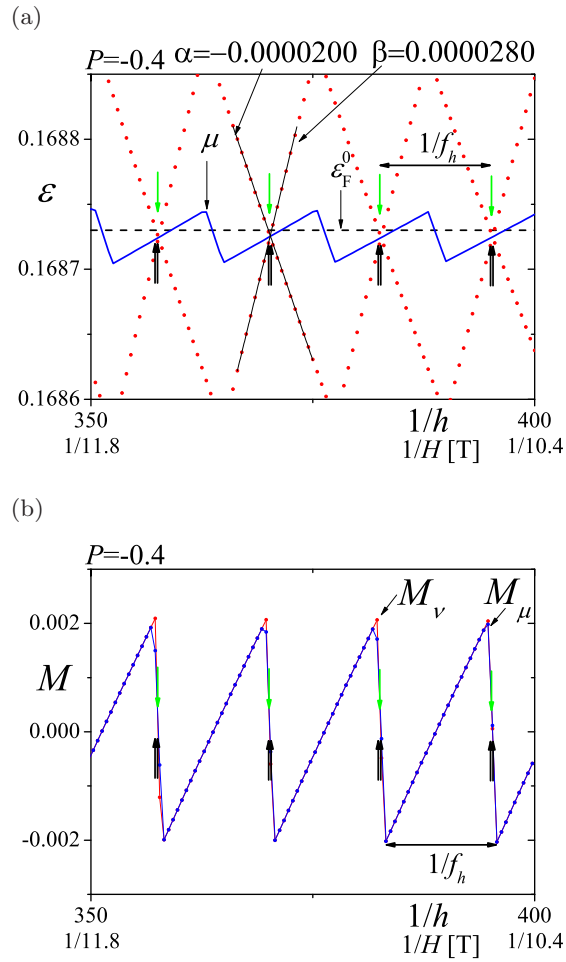

FIG. 11. (a) Energy as a function of $1/h$ [an enlarged view in the region near ε_F^0 and small h in Fig. 6(a) plotted ε as a function of $1/h$]. (b) The enlarged figures of M_ν (a red line) in Fig. 9(a) and M_μ (a blue line) in Fig. 10(a) in the same region of $1/h$ as (a). The green arrows in (a) are the crossing points of the chemical potential (for fixed ν, a blue line) and the red dotted lines [Landau levels of the electron pockets (negatively sloped lines) and those of the hole pockets (positively sloped lines)]. The red dotted lines for the hole pockets or the electron pockets are almost parallel in this enlarged figure, respectively. The Landau levels can be approximated as straight lines [a negatively sloped black line and a positively sloped black line in (a)]. The slopes of Landau levels of the electron pocket are $\alpha = -0.0000200$ and those of the hole pocket are $\beta = 0.0000280$. The black arrows in (a) are the crossing points of the chemical potential (for fixed μ, a black dotted line) and the red dotted lines. Note that four lines cross almost simultaneously. The spacings of the green arrows are the same and $1/f_h$. Therefore, there appear in M_ν and M_μ the dHvA oscillations with the fundamental frequency of f_h, which corresponds to the area of the hole pocket (equal to that of the electron pocket). Due to the difference of the density of states of electrons (fourth band) and holes (third band) [see Fig. 4(a)], the absolute values of the slopes ($|\alpha|$ and $|\beta|$) in the electron pocket's Landau levels and the hole pocket's Landau levels are different.

shown in Fig. 3(c). The large peaks at $f_h/2$ in M_ν and M_μ also appear, which corresponds to the area $[A_e/(2A_{BZ}) \simeq 0.0333]$ of a small electron pocket. These are expected in the LK formula. Moreover, there are peaks at $3f_h/2$, $5f_h/2$, and $7f_h/2$ in Fig. 15(c). These peaks might be explained by the network model for the magnetic breakdown.

Note that the peaks at $3f_h/2$ and $5f_h/2$ in M_ν are large, whereas these are very small in M_μ, as shown in Fig. 15(c).

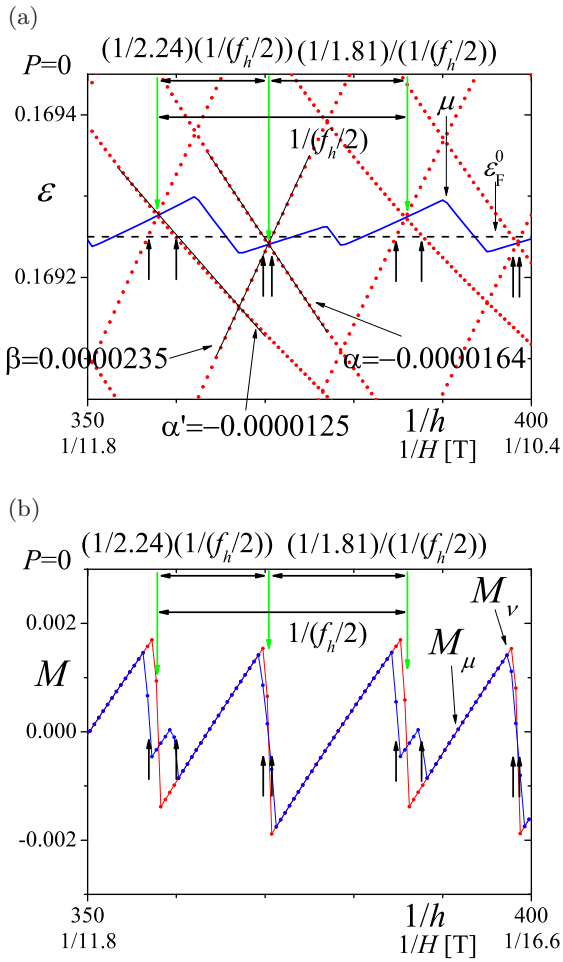

FIG. 12. The same figures as Fig. 11 at $P = 0$, where there is a narrow neck in the electron pocket. The Landau levels of the electron pocket with the slope α and with α' (negatively sloped lines) are not parallel to each other, but the Landau levels of the electron pocket with the same slope value are parallel. The Landau levels of the hole pocket (positively sloped lines) are also parallel to each other. The values of slopes are $\alpha = -0.0000164$, $\alpha' = -0.0000125$, and $\beta = 0.0000235$, respectively [see (a)]. The spacing of $1/(f_h/2)$ of the green arrows is periodical. Similarly, one pattern of four crossings of ε_F^0 and the Landau levels (four black arrows) is repeated periodically with $1/(f_h/2)$. As a result, there appear in M_ν and M_μ the dHvA oscillations with the fundamental frequency of $f_h/2$, which corresponds to the half area of the hole pocket [equal to the area of green regions of the electron pocket in Fig. 3(b)]. Since the Landau levels due to electron pockets are not parallel, jumps in M_ν (green arrows) and M_μ (black arrows) occur at incommensurate points in the period $[1/(f_h/2)]$ [see (b)]. These incommensurate jumps in M_ν and M_μ mean that the FTIs are not given by a simple function of f.

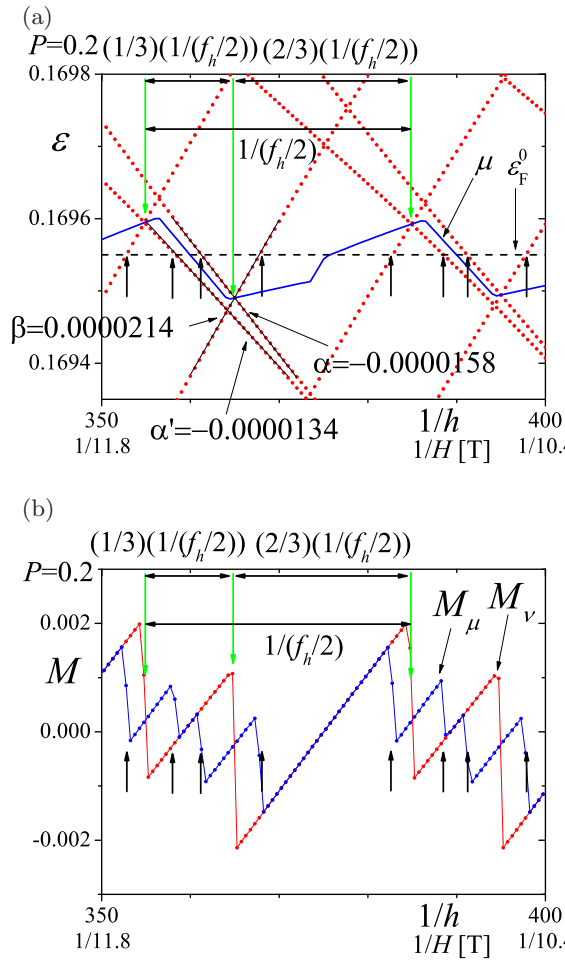

FIG. 13. The same figures as Fig. 11 at $P = 0.2$, where two electron pockets are separated by narrow region in the momentum space [close to the Lifshitz transition, see Fig. 3(c)]. The slope of the Landau levels are $\alpha = -0.0000158$, $\alpha' = -0.0000134$, and $\beta = 0.0000214$, respectively [see (a)]. The Landau levels of the electron pockets come near as a pair but there is the small difference within the pair. This situation can be interpreted as the almost degenerate Landau levels in two electron pockets couple via tunneling (magnetic breakdown in other word). Although the electron pockets' Landau levels with α and α' are not parallel to each other, small lifting of the degeneracy of the electron pockets' Landau levels makes the almost-commensurate separation of the green arrows at $1/3 : 2/3$. As a result, the jumps in M_ν occur at commensurate point $[(1/3)(1/(f_h/2))]$ in the period $[1/(f_h/2)]$, whereas jumps in M_μ occur at $(1/2)(1/(f_h/2))$ and incommensurate points [see (b)]. This fact explains why $3f_h/2$ frequency of the dHvA oscillations is enhanced when ν is fixed, but not when μ is fixed.

The peaks at $3f_h/2$ and $5f_h/2$ are maximized at $P = 0.2$ and $P = 0.1$ (near the Lifshitz transition), respectively, as shown in Fig. 1. We consider that the enhancement of the peak at $3f_h/2$ in M_ν is closely related to the periodicities of the crossings (green arrows) of the Landau levels and μ in Figs. 12–14.

The fundamental period of $1/(f_h/2)$ in M_ν at $P = 0$ and 0.2 comes from the crossings of every second negatively sloped line, every second positively sloped line, and μ. At $P = 1.0$, it comes from the crossings of every negatively sloped line, every second positively sloped line, and μ, where negatively sloped lines (electron pocket's Landau levels) are effectively degenerated doubly. That fundamental period is divided into two periods $[(1/2.24)(1/(f_h/2))$ and $(1/1.81)(1/(f_h/2))$ in Fig. 12, $(1/3)(1/(f_h/2))$ and $(2/3)(1/(f_h/2))$ in Fig. 13, and $(1/4.82)(1/(f_h/2))$ and $(1/1.81)(1/(f_h/2))$ in Fig. 14]. These two periods are changed by the spacing of the separations of negatively sloped lines. When $P = 0.2$, the ratio of two periods $(1/3 : 2/3)$ is a simple one, as shown in Fig. 13. Then,

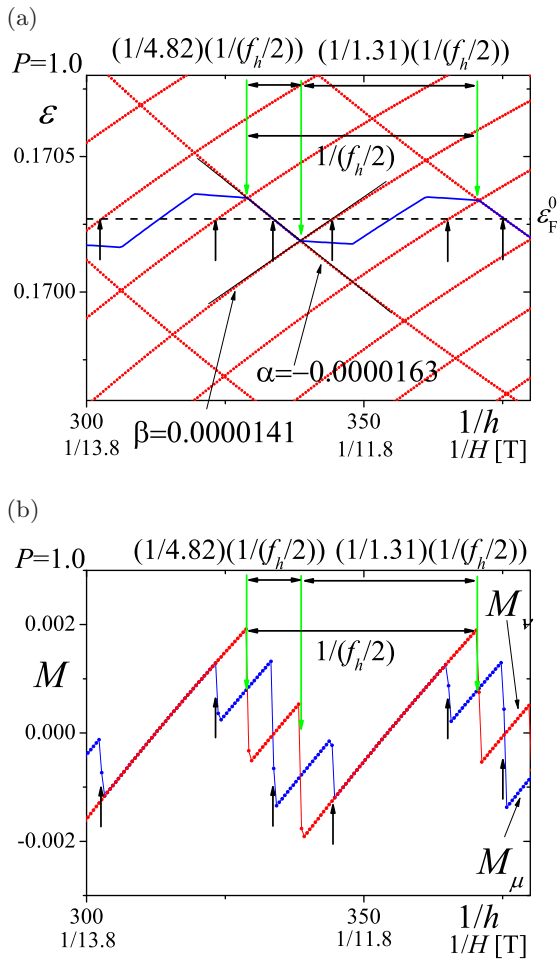

FIG. 14. The same figures as Fig. 11 at $P = 1.0$, where two electron pockets are separated enough in the momentum space [see Fig. 3(d)]. The Landau levels of the electron pockets are degenerated as a pair in this scale of figures. The absolute value of the slope ($|\alpha| = 0.0000141$) of the electron pockets' Landau levels is smaller than that ($|\beta| = 0.0000163$) of the hole pocket's Landau levels. Jumps in M_ν and M_μ occur at incommensurate points in the period $[1/(f_h/2)]$ [see (b)].

the FTI at $3f_h/2$ in M_ν becomes large. This is explained in Appendix D. Thus, the enhancement of $3f_h/2$ near the Lifshitz transition is caused by the commensurate separation of the Landau levels. On the other hand, since the separation of the electron pockets' Landau levels hardly affects the fundamental period of $1/(f_h/2)$, the FTI at $f_h/2$ is not maximized near the Lifshitz transition.

At $P = 1.0$, there is a large peak at $f_h/2 \simeq 0.0239$ in the FTIs [Fig. 15(d)]. This frequency corresponds to each area of an electron pocket $[A_e/(2A_{\rm BZ}) \simeq 0.0240]$ in Fig. 3(d). Note that the peaks at f_h and $3f_h$ in M_ν and M_μ are very small, as shown in Fig. 15(d).

We have already found [32] the smallness of these peaks in M_μ. In that paper, we could not explain the smallness, which would be large in the LK formula with free electrons. Here, we show that the smallness can be explained by the LK formula with the difference of the phase factors for the electron pockets and a hole pocket. The phase factor for a hole pocket

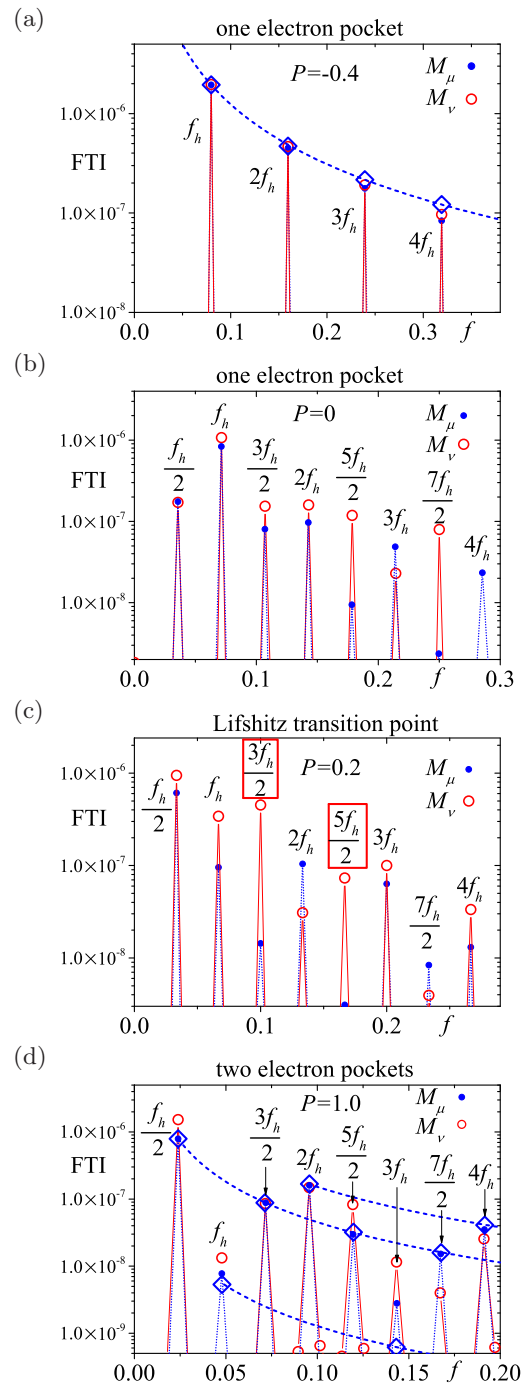

FIG. 15. The FTIs of M_ν and M_μ for at $P = -0.4$ (one electron pocket) (a), $P = 0$ (one electron pocket) (b), $P = 0.2$ (Lifshitz transition point) (c), and $P = 1.0$ (two electron pockets) (d). The regions of the Fourier transform are $200 \leqslant 1/h \leqslant 388$ in (a), $202.75 \leqslant 1/h \leqslant 398.75$ for M_ν and $203.25 \leqslant 1/h \leqslant 399.25$ for M_μ in (b), $215.75 \leqslant 1/h \leqslant 395.25$ for M_ν and $218.25 \leqslant 1/h \leqslant 398.25$ for M_μ in (c), and $213.5 \leqslant 1/h \leqslant 381$ for M_ν and $209.25 \leqslant 1/h \leqslant 376.5$ for M_μ in (d). In (a) and (d), blue diamonds are the FTIs of the LK formula. The dotted blue lines are the guides to the eye. In (c), the FTIs at $3f_h/2$ and $5f_h/2$ are enhanced.

is $\gamma_h = 1/2$, as in the usual free holes with parabolic energy dispersion, whereas that for two electron pockets is $\gamma_e = 0$, which is the cases in the Dirac fermions [77]. Since the system

is overtilted Dirac fermions at $P = 1.0$, taking $\gamma_e = 0$ is not completely justified but it is plausible to take $\gamma_e = 0$ due to not opening the gap at the Dirac points. Then, the LK formula for $P = 1.0$ is given by Eq. (E3) in Appendix E. By using the value of $D_4(\varepsilon_F^0)/D_3(\varepsilon_F^0)$ in Fig. 4(d), we obtain $\widetilde{A}_h/\widetilde{A}_e = 0.832$ from Eq. (E6). In that case, by setting the value of the FTI at $f_h/2$ in M_μ as $|M_0\widetilde{A}_e|^2$, we can determine the values of Eqs. (E4) and (E5), which are indicated by the blue diamonds in Fig. 15(d). These almost coincide with the FTIs at $f_h/2$, $3f_h/2$, $2f_h$, $5f_h/2$, $7f_h/2$, and $4f_h$ in M_μ. However, the FTIs at f_h and $3f_h$ are deviated from these fitting (blue diamonds). We guess that the deviations at f_h and $3f_h$ may be due to the magnetic breakdown or the numerical errors.

VI. CONCLUSIONS

We study the dHvA oscillations in the two-dimensional compensated metal with overtilted Dirac cones near the Lifshitz transition by using the tight-binding model of α-(BEDT − TTF)$_2$I$_3$. It is shown that in this system the dHvA oscillations under the condition of the fixed electron number are caused by the periodical crossings of the Landau levels and the chemical potential. This is in contrast with the dHvA oscillations in the two-dimensional free electrons whose origin is periodical jumps of the chemical potential.

At $P \sim 0.2$ kbar and 10.4 T $\leqslant H \leqslant$ 20.7 T, we find the enhancements of the dHvA oscillations with the frequencies of $3f_h/2$ and $5f_h/2$ under the condition of the fixed electron number. These enhancements happen in the pressure region where the topology of the Fermi surface changes from one electron pocket to two electron pockets (Lifshitz transition). These enhancements are caused by the commensurate separation of two Landau levels with the phase factor ($\gamma_e \simeq 0$) seen in Dirac fermions. These will be observed in the two-dimensional overtilted Dirac fermions if the situation near the Lifshitz transition is realized by applying the pressures, doping, etc.

APPENDIX A: LIFSHITZ AND KOSEVICH FORMULA

Although the magnetization should be calculated under the condition of the fixed electron number or the fixed electron filling, ν, (canonical ensemble), Lifshitz and Kosevich [2] have calculated it under the condition of the fixed chemical potential, μ, (grand canonical ensemble). This is because the calculation in the grand canonical ensemble is justified if μ does not depend on the magnetic field or depends very weakly on the magnetic field.

They have derived the LK formula [1–3] for the free electron model by using the semiclassical quantization rule [76]. Recently, it has been also shown that the LK formula can be used for the Dirac fermions [34–36]. The LK formula at $T = 0$ for the two-dimensional multi closed Fermi surface with the area (A_i) is given by

$$M^{\mathrm{LK}} = M_0 \sum_i \widetilde{A}_i \sum_{l=1}^{\infty} \frac{1}{l} \sin\left[2\pi l\left(\frac{F_i}{H} - \gamma_i\right)\right], \quad \text{(A1)}$$

$$M_0 = -\frac{e}{2\pi^2 c\hbar}, \quad \text{(A2)}$$

$$\widetilde{A}_i = \frac{|A_i|}{\frac{\partial A_i(\varepsilon^0)}{\partial \varepsilon^0}\big|_{\varepsilon^0=\mu}}, \quad \text{(A3)}$$

where i is the index for the closed orbit and the frequency (F_i) is given by

$$F_i = \frac{c\hbar|A_i|}{2\pi e}, \quad \text{(A4)}$$

where $A_i > 0$ and $A_i < 0$ are for the electron pocket and the hole pocket, respectively. Note that $\widetilde{A}_i$ is positive both for the electron pocket and for the hole pocket in the situation studied in this paper. When we use h instead of H in Eq. (A1), we get

$$\frac{F_i}{H} = \frac{f_i}{h}, \quad \text{(A5)}$$

where

$$f_i = \frac{|A_i|}{A_{\mathrm{BZ}}}. \quad \text{(A6)}$$

In Eq. (A1), γ_i is the phase of the oscillation, which comes from the phase of the Landau levels. For example, $\gamma = 1/2$ and $\gamma = 0$ are for the free electron model and the Dirac fermions [77], respectively. We consider the case of the single free electron pocket with the area of A_e. Eq. (A3) becomes

$$M^{\mathrm{LK}} = M_0\widetilde{A}_e \sum_{l=1}^{\infty} \frac{1}{l} \sin\left[2\pi l\left(\frac{F_e}{H} - \frac{1}{2}\right)\right]. \quad \text{(A7)}$$

Under the condition of the fixed ν, the highest Landau level is partially filled, i.e., μ is pinned at the Landau level at $T = 0$, as shown in Fig. 16(a). As the magnetic field is increased, the degeneracy of each Landau level increases, and μ jumps periodically as a function of $1/H$. These jumps are the origins of the dHvA oscillations. Under the condition of fixed μ, the Landau levels and μ crosses periodically. Then, the dHvA oscillations appear, as shown in Fig. 16(b). The wave form of M_ν is inverted from that of M_μ [Eq. (A7)].

APPENDIX B: FOURIER TRANSFORM INTENSITIES

To analyze the oscillations in the magnetization, we calculate the FTIs numerically as follows. By choosing the center (h_c) and the finite range ($2L$), we calculate

$$\mathrm{FTI}\left(f, \frac{1}{h_c}, L\right) = \left|\frac{1}{2L}\int_{\frac{1}{h_c}-L}^{\frac{1}{h_c}+L} M(h) e^{2\pi i \frac{f}{h}} d\left(\frac{1}{h}\right)\right|^2, \quad \text{(B1)}$$

where we take $f = j/(2L)$ with integer j ($0 \leqslant j \leqslant 256$ is used in this paper).

For example, in the system with one electron pocket, from Eq. (A7) the FTIs at $f_e, 2f_e, 3f_e, \ldots$ in M^{LK} become

$$\mathrm{FTI}(f = lf_e) = \left|\frac{M_0\widetilde{A}_e}{l}\right|^2, \quad \text{(B2)}$$

where $l = 1, 2, 3, \ldots$.

APPENDIX C: THE TIME-REVERSAL INVARIANT MOMENTUM

The TRIM, $\mathbf{p}_{\mathrm{TRIM}} = \hbar\mathbf{k}_{\mathrm{TRIM}}$, is given by the reciprocal lattice vectors ($\mathbf{G}_j$), where $j = 1, 2$ ($j = 1, 2, 3$) if we study a two-dimensional system (a three-dimensional system), as

$$\mathbf{k}_{\mathrm{TRIM}} = \sum_j \frac{1}{2} n_j \mathbf{G}_j, \quad \text{(C1)}$$

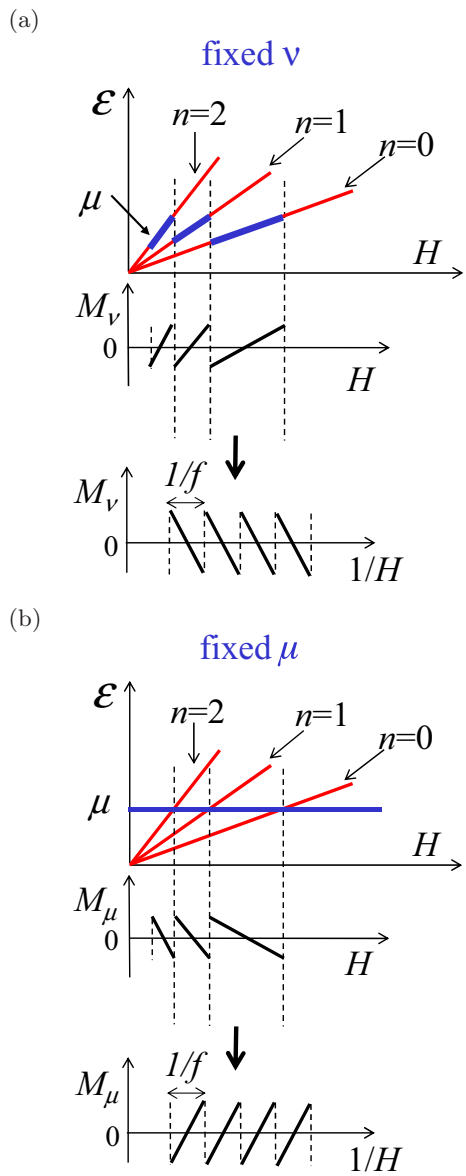

FIG. 16. In the two-dimensional system with an electron pocket, schematic figures of the Landau levels (red lines), the chemical potential (blue lines) and the dHvA oscillations (black lines). (a) and (b) are for the conditions of the fixed electron number and of the fixed chemical potential, respectively.

where $n_j = 0$ or 1. In the two-dimensional system there are four TRIMs in the first Brillouin zone. Note that $\mathbf{k}_{\rm TRIM}$ and $-\mathbf{k}_{\rm TRIM}$ are equivalent. We study the system having the inversion symmetry, i.e.,

$$\hat{\mathcal{H}} = \hat{P}\hat{\mathcal{H}}\hat{P}^{-1}, \tag{C2}$$

where $\hat{P}$ is the parity operator and $\hat{P}^{-1} = \hat{P}$ and $\hat{\mathcal{H}}$ is the Hamiltonian. The eigenstate and the energy are given by

$$\hat{\mathcal{H}}|\mathbf{k}\rangle = \epsilon_{\mathbf{k}}|\mathbf{k}\rangle. \tag{C3}$$

By using Eq. (C2), we obtain

$$\hat{\mathcal{H}}|\mathbf{k}\rangle = \hat{P}\hat{\mathcal{H}}\hat{P}^{-1}|\mathbf{k}\rangle, \tag{C4}$$

$$= \hat{P}\hat{\mathcal{H}}|-\mathbf{k}\rangle, \tag{C5}$$

$$= \hat{P}\epsilon_{-\mathbf{k}}|-\mathbf{k}\rangle, \tag{C6}$$

$$= \epsilon_{-\mathbf{k}}|\mathbf{k}\rangle. \tag{C7}$$

From Eqs. (C3) and (C7), we obtain

$$\epsilon_{\mathbf{k}} = \epsilon_{-\mathbf{k}}. \tag{C8}$$

We assume that the energy band $|\mathbf{k}\rangle$ does not cross the other band at the TRIMs. This assumption is not satisfied when a spin-orbit coupling is taken into account in the system having the time-reversal symmetry. Here we have employed the model neglecting the spin as well as the spin-orbit coupling. It means that the band is simply doubled and the result is not changed if the spin is taken into account.

The gradient of the band at $\mathbf{k}$ and $-\mathbf{k}$ is obtained as

$$\nabla\epsilon_{-\mathbf{k}} = \lim_{\delta\mathbf{k}\to\mathbf{0}} \frac{\epsilon_{-\mathbf{k}+\delta\mathbf{k}} - \epsilon_{-\mathbf{k}}}{\delta\mathbf{k}}, \tag{C9}$$

$$= \lim_{\delta\mathbf{k}\to\mathbf{0}} \frac{\epsilon_{\mathbf{k}-\delta\mathbf{k}} - \epsilon_{\mathbf{k}}}{\delta\mathbf{k}}, \tag{C10}$$

$$= -\nabla\epsilon_{\mathbf{k}}, \tag{C11}$$

i.e.,

$$\nabla\epsilon_{\mathbf{k}} = -\nabla\epsilon_{-\mathbf{k}}. \tag{C12}$$

Therefore, if the band does not cross the other band at $\mathbf{k} = \mathbf{0}$, we obtain

$$\nabla\epsilon_{\mathbf{0}} = -\nabla\epsilon_{\mathbf{0}} = 0. \tag{C13}$$

Similarly, by using

$$\epsilon_{\mathbf{k}_{\rm TRIM}+\mathbf{q}} = \epsilon_{\mathbf{k}_{\rm TRIM}-\mathbf{q}}, \tag{C14}$$

we obtain

$$\nabla\epsilon_{\mathbf{k}_{\rm TRIM}} = 0. \tag{C15}$$

We conclude that if the system has the inversion symmetry, the TRIM may become any of a local maximum point, a local minimum point, an inflection point, or a saddle point.

APPENDIX D: AMPLITUDES OF FOURIER COEFFICIENTS OF THE SAW-TOOTH WAVE

The sawtooth dependence with period $1/(f/2)$ of the magnetization as a function of $1/h = x$ is given by

$$M^0(x) = cx \quad \text{if } -\frac{1}{f} < x < \frac{1}{f} \tag{D1}$$

and

$$M^0(x) = M^0\left(x + \frac{2m}{f}\right), \quad m = \pm1, \pm2, \ldots, \tag{D2}$$

where c is a constant.

The sawtooth function, $M^0(x)$, is given by the Fourier series as

$$M^0(x) = a_0^0 + \sum_{\ell=1}^{\infty}\left[a_\ell^0 \cos\left(2\pi\ell\frac{f}{2}x\right) + b_\ell^0 \sin\left(2\pi\ell\frac{f}{2}x\right)\right], \tag{D3}$$

where the coefficients, a_ℓ^0 and b_ℓ^0, are given by

$$a_\ell^0 = 0, \tag{D4}$$

$$b_\ell^0 = \frac{2c}{f\pi}\frac{(-1)^{\ell+1}}{\ell}. \tag{D5}$$

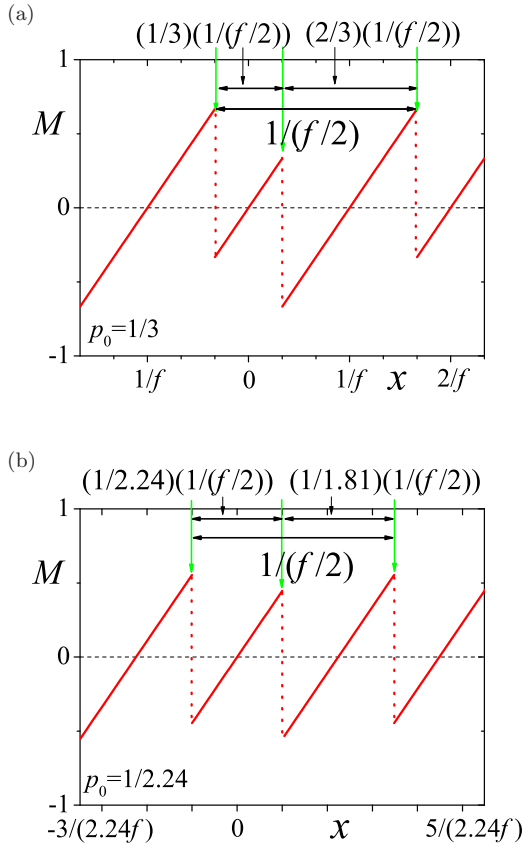

FIG. 17. $M(x)$ as a function of x at $p_0 = 1/3$ (a) and at $p_0 = 1/2.24$ (b), where we take $c = 1$ and $q_0 = 1$.

We now consider the modified saw-tooth dependence

$$M(x) = \begin{cases} cx, & \text{if } -\frac{p_0}{f} < x < \frac{p_0}{f} \\ c\left(x - \frac{q_0}{f}\right), & \text{if } \frac{p_0}{f} < x < \frac{2-p_0}{f} \end{cases} \tag{D6}$$

where we set $0 < p_0 \leqslant 1$, as shown in Figs. 17(a) and 17(b). Then, we obtain

$$a_0 = \frac{2c(1-p_0)(1-q_0)}{f}, \tag{D7}$$

$$a_\ell = -\frac{2c(1-q_0)}{f\ell\pi}\sin(\ell p_0\pi), \tag{D8}$$

and

$$b_\ell = -\frac{2c}{f\ell\pi}\cos(\ell p_0\pi). \tag{D9}$$

If $q_0 = 1$, we obtain $a_0 = a_\ell = 0$ and only sine components exist. In this case ($q_0 = 1$), $|b_3|$ in Eq. (D9) is maximized at $p_0 = 1/3$ and $2/3$. When $p_0 = 1/3$, the fundamental period $[1/(f/2)]$ is divided into $(1/3)(1/(f/2))$ and $(2/3)(1/(f/2))$, as shown in Fig. 17(a). When $p_0 = 1/2.24$, the fundamental period is divided into $(1/2.24)(1/(f/2))$ and $(1/1.81)(1/(f/2))$, as shown in Fig. 17(b). Similar situations are realized in M_v at $P = 0$, 0.2, and 1.0 [see Figs. 12(b), 13(b), and 14(b)]. The sawtooth pattern of M_v is modified commensurately ($p_0 = 1/3$) at $P = 0.2$ near the Lifshitz transition, but incommensurately at $P = 0$ and 1.0. Therefore, the FTI at $3f_h/2$ in M_v, which is proportional to $|b_3|^2$, is enhanced at $P = 0.2$.

APPENDIX E: LK FORMULA WITH A HOLE POCKET AND TWO SMALL ELECTRON POCKETS

We consider the case of one hole pocket with the area of $|A_h|$ and two same electron pockets with each area of $A_e/2$, where $A_e = |A_h|$. If we ignore the effect of the magnetic breakdown, the LK formula of Eq. (A1) becomes

$$\frac{M^{\rm LK}}{M_0} = \widetilde{A}_h \sum_{l=1}^{\infty}\frac{1}{l}\sin\left[2\pi l\left(\frac{f_h}{h} - \gamma_h\right)\right] + 2\widetilde{A}_e\sum_{l=1}^{\infty}\frac{1}{l}\sin\left[2\pi l\left(\frac{f_h}{2h} - \gamma_e\right)\right], \tag{E1}$$

where we set $f_e/2 = f_h/2$ for two electron pockets. By putting $\gamma_h = 1/2$ and $\gamma_e = 0$ into Eq. (E1), we obtain

$$\frac{M^{\rm LK}}{M_0} = \widetilde{A}_h \sum_{l=1}^{\infty}(-1)^l\frac{1}{l}\sin\left[2\pi l\left(\frac{f_h}{h}\right)\right] + 2\widetilde{A}_e\sum_{l=1}^{\infty}\frac{1}{l}\sin\left[2\pi l\left(\frac{f_h}{2h}\right)\right] \tag{E2}$$

$$= \widetilde{A}_e\sum_{m=1}^{\infty}\left\{\left[(-1)^m\left(\frac{\widetilde{A}_h}{\widetilde{A}_e}\right)+1\right]\frac{1}{m}\sin\left[2\pi m\left(\frac{f_h}{h}\right)\right] + \frac{2}{2m-1}\sin\left[2\pi(2m-1)\left(\frac{f_h}{2h}\right)\right]\right\}. \tag{E3}$$

From Eq. (E3), the FTIs are given by

$$\mathrm{FTI}(f = mf_h) = \left|\frac{M_0\widetilde{A}_e}{m}\left[(-1)^m\left(\frac{\widetilde{A}_h}{\widetilde{A}_e}\right)+1\right]\right|^2, \tag{E4}$$

$$\mathrm{FTI}\left(f = m\frac{f_h}{2}\right) = \left|\frac{2M_0\widetilde{A}_e}{2m-1}\right|^2, \tag{E5}$$

where $m = 1, 2, 3, \ldots$.

Since the density of states is proportional to $\partial A_i(\varepsilon^0)/\partial\varepsilon^0$, by using Eq. (A3) we obtain

$$\frac{\widetilde{A}_h}{\widetilde{A}_e} = \frac{|A_h|}{\frac{\partial A_h(\varepsilon^0)}{\partial\varepsilon^0}\big|_{\varepsilon^0=\mu}}\frac{\frac{\partial A_e(\varepsilon^0)}{\partial\varepsilon^0}\big|_{\varepsilon^0=\mu}}{|A_e|} = \frac{D_4(\varepsilon^0)}{D_3(\varepsilon^0)}. \tag{E6}$$

In a special case of $\widetilde{A}_h/\widetilde{A}_e = 1$ in Eq. (E4), the FTIs at f_h, $3f_h$, $5f_h$, … vanish.

[1] D. Schoenberg, *Magnetic Oscillation in Metals* (Cambridge University Press, Cambridge, 1984).
[2] I. M. Lifshitz and A. M. Kosevich, Zh. Eksp. Teor. Fiz. **29**, 730 (1955) [Sov. Phys. JETP **2**, 636 (1956)].
[3] T. Champel and V. P. Mineev, Philos. Mag. B **81**, 55 (2001).
[4] A. B. Pippard, Proc. Roy. Soc. (London) **A270**, 1 (1962).
[5] L. M. Falicov and H. Stachoviak, Phys. Rev. **147**, 505 (1966).
[6] T. Champel, Phys. Rev. B **64**, 054407 (2001).

[7] P. D. Grigoriev, J. Exp. Theor. Phys. **92**, 1090 (2001).
[8] F. A. Meyer, E. Steep, W. Biberacher, P. Christ, A. Lerf, A. G. M. Jansen, W. Joss, P. Wyder, and K. Andres, Europhys. Lett. **32**, 681 (1995).
[9] N. Harrison, J. Caulfield, J. Singleton, P. H. P. Reinders, F. Herlach, W. Hayes, M. Kurmoo, and P. Day, J. Phys.: Condens. Matter **8**, 5415 (1996).
[10] S. Uji, M. Chaparala, S. Hill, P. S. Sandhu, J. Qualls, L. Seger, and J. S. Brooks, Synth. Met. **85**, 1573 (1997).
[11] E. Steep, L. H. Nguyen, W. Biberacher, H. Muller, A. G. M. Jansen, and P. Wyder, Physica B **259–261**, 1079 (1999).
[12] M. M. Honold, N. Harrison, M. S. Nam, J. Singleton, C. H. Mielke, M. Kurmoo, and P. Day, Phys. Rev. B **58**, 7560 (1998).
[13] A. Audouard, D. Vignolles, E. Haanappel, I. Sheikin, R. B. Lyubovskii, and R. N. Lyubovskaya, Europhys. Lett. **71**, 783 (2005).
[14] A. Audouard and J. Y. Fortin, C. R. Phys. **14**, 15 (2013).
[15] M. Nakano, J. Phys. Soc. Jpn. **66**, 19 (1997).
[16] A. S. Alexandrov and A. M. Bratkovsky, Phys. Rev. Lett. **76**, 1308 (1996).
[17] A. S. Alexandrov and A. M. Bratkovsky, Phys. Rev. B **63**, 033105 (2001).
[18] T. Champel, Phys. Rev. B **65**, 153403 (2002).
[19] K. Kishigi and Y. Hasegawa, Phys. Rev. B **65**, 205405 (2002).
[20] M. A. Itskovsky, Phys. Rev. B **68**, 054423 (2003).
[21] V. M. Gvozdikov, A. G. M. Jansen, D. A. Pesin, I. D. Vagner, and P. Wyder, Phys. Rev. B **68**, 155107 (2003).
[22] K. Machida, K. Kishigi, and Y. Hori, Phys. Rev. B **51**, 8946 (1995).
[23] K. Kishigi, M. Nakano, K. Machida, and Y. Hori, J. Phys. Soc. Jpn. **64**, 3043 (1995).
[24] K. Kishigi, J. Phys. Soc. Jpn. **66**, 910 (1997).
[25] P. S. Sandhu, J. H. Kim, and J. S. Brooks, Phys Rev. B **56**, 11566 (1997).
[26] J. Y. Fortin and T. Ziman, Phys. Rev. Lett. **80**, 3117 (1998).
[27] S. Y. Han, J. S. Brooks, and J. H. Kim, Phys. Rev. Lett. **85**, 1500 (2000).
[28] V. M. Gvozdikov, A. G. M. Jansen, D. A. Pesin, I. D. Vagner, and P. Wyder, Phys. Rev. B **70**, 245114 (2004).
[29] For a review, see T. Ishiguro, K. Yamaji, and G. Saito, *Organic Superconductors*, 2nd ed. (Springer-Verlag, Berlin, 1998).
[30] For a review, see *The Physics of Organic Superconductors and Conductors*, edited by A. G. Lebed (Springer, Berlin, 2008).
[31] S. Katayama, A. Kobayashi, and Y. Suzumura, J. Phys. Soc. Jpn. **75**, 054705 (2006).
[32] K. Kishigi and Y. Hasegawa, Phys. Rev. B **96**, 085430 (2017).
[33] Y. Hasegawa and K. Kishigi, Phys. Rev. B **99**, 045409 (2019)
[34] I. A. Luk'yanchuk and Y. Kopelevich, Phys. Rev. Lett. **93**, 166402 (2004).
[35] I. A. Luk'yanchuk, J. Low Temp. Phys. **37**, 45 (2011).
[36] S. G. Sharapov, V. P. Gusynin, and H. Beck, Phys. Rev. B **69**, 075104 (2004).
[37] J. Y. Fortin and A. Audouard, Phys. Rev. B **77**, 134440 (2008).
[38] J. Y. Fortin and A. Audouard, Phys. Rev. B **80**, 214407 (2009).
[39] K. Kishigi and K. Machida, Phys. Rev. B **53**, 5461 (1996).
[40] K. Kishigi and Y. Hasegawa, Phys. Rev. B **94**, 085405 (2016).
[41] J. P. Pouget, R. Moret, R. Comes, and K. Bechgaard, J. Phys. Lett. (France) **42**, 543 (1981).
[42] D. Vignolles, A. Audouard, M. Nardone, and L. Brossard, S. Bouguessa, and J. M. Fabre, Phys. Rev. B **71**, 020404(R) (2005).
[43] W. Kang and O.-H. Chung, Phys. Rev. B **79**, 045115 (2009).
[44] I. M. Lifshitz, Zh. Eksp. Teor. Fiz. **38**, 1569 (1960) [Sov. Phys. JETP **11**, 1130 (1960)].
[45] G. E. Volovik, J. Low Temp. Phys. **43**, 47 (2017).
[46] A. A. Soluyanov, D. Gresch, Z. Wang, Q. Wu, M. Troyer, X. Dai, and B. A. Bernevig, Nature (London) **527**, 495 (2015).
[47] Z. M. Yu, Y. Yao, and S. A. Yang, Phys. Rev. Lett. **117**, 077202 (2016).
[48] In the two-dimensional metallic system including the spin, Itskovsky and Maniv [49] have succeeded to take the van Hove singularity into the semiclassical calculation by using the approximation by Zil'berman [50, 51]. They have shown that the dHvA oscillation is different from the LK formula.
[49] M. A. Itskovsky and T. Maniv, Phys. Rev. B **72**, 075124 (2005).
[50] G. E. Zil'berman, Zh. Eksp. Teor. Fiz. **34**, 515 (1958) [Sov. Phys. JETP **7**, 355 (1958)].
[51] G. E. Zil'berman, Zh. Eksp. Teor. Fiz. **32**, 296 (1957) [Sov. Phys. JETP **5**, 208 (1957)].
[52] K. Kajita, Y. Nishio, N. Tajima, Y. Suzumura, and A. Kobayashi, J. Phys. Soc. Jpn. **83**, 072002 (2014).
[53] H. Kino and H. Fukuyama, J. Phys. Soc. Jpn. **64**, 1877 (1995).
[54] H. Seo, J. Phys. Soc. Jpn. **69**, 805 (2000).
[55] Y. Takano, K. Hiraki, H. M. Yamamoto, T. Nakamura, and T. Takahashi, J. Phys. Chem. Solids **62**, 393 (2001).
[56] R. Wojciechowski, K. Yamamoto, K. Yakushi, M. Inokuchi, and A. Kawamoto, Phys. Rev. B **67**, 224105 (2003).
[57] N. Tajima, A. Ebina-Tajima, M. Tamura, Y. Nishio, and K. Kajita, J. Phys. Soc. Jpn. **71**, 1832 (2002).
[58] N. Tajima, T. Yamauchi, T. Yamaguchi, M. Suda, Y. Kawasugi, H. M. Yamamoto, R. Kato, Y. Nishio, and K. Kajita, Phys. Rev. B **88**, 075315 (2013).
[59] R. Beyer, A. Dengl, T. Peterseim, S. Wackerow, T. Ivek, A. V. Pronin, D. Schweitzer, and M. Dressel, Phys. Rev. B **93**, 195116 (2016).
[60] D. Liu, K. Ishikawa, R. Takehara, K. Miyagawa, M. Tamura, and K. Kanoda, Phys. Rev. Lett. **116**, 226401 (2016).
[61] M. V. Kartsovnik, V. N. Zverev, D. Andres, W. Biberacher, T. Helm, P. D. Grigoriev, R. Ramazashvili, N. D. Kushch, and H. Muller, Low Temp. Phys. **40**, 377 (2014).
[62] K. Kajita, T. Ojiro, H. Fujii, Y. Nishio, H. Kobayashi, A. Kobayashi, and R. Kato, J. Phys. Soc. Jpn. **61**, 23 (1992).
[63] N. Tajima, M. Tamura, Y. Nishio, K. Kajita, and Y. Iye, J. Phys. Soc. Jpn. **69**, 543 (2000)
[64] M. Hirata, K. Ishikawa, K. Miyagawa, K. Kanoda, and M. Tamura, Phys. Rev. B **84**, 125133 (2011).
[65] T. Konoike, K. Uchida, and T. Osada, J. Phys. Soc. Jpn. **81**, 043601 (2012).
[66] T. Osada, J. Phys. Soc. Jpn. **77**, 084711 (2008).
[67] A. Kobayashi, S. S. Katayama, K. Noguchi, and Y. Suzumura, J. Phys. Soc. Jpn. **73**, 3135 (2004).
[68] T. Mori, A. Kobayashi, Y. Sasaki, H. Kobayashi, G. Saito, and H. Inokuchi, Chem. Lett. **13**, 957 (1984).
[69] R. Kondo, S. Kagoshima, and J. Harada, Rev. Sci. Instrum. **76**, 093902 (2005).
[70] H. Kino and T. Miyazaki, J. Phys. Soc. Jpn. **75**, 034704 (2006).

[71] H. Kino and T. Miyazaki, J. Phys. Soc. Jpn. **78**, 105001 (2009).
[72] P. Alemany, J. P. Pouget, and E. Canadell, Phys. Rev. B **85**, 195118 (2012).
[73] M. Nakano, Phys. Rev. B **62**, 45 (2000).
[74] P. G. Harper, Proc. Phys. Soc. Lond. A **68**, 874 (1955).
[75] G. Montambaux, F. Piechon, J. N. Fuchs, and M. O. Goerbig, Eur. Phys. J. B **72**, 509 (2009).
[76] L. Onsager, Philos. Mag. **43**, 1006 (1952).
[77] G. P. Mikitik and Yu. V. Sharlai, Phys. Rev. Lett. **82**, 2147 (1999).